Article:
Luo, W., Wang, Z., Lu, J. et al. (4 more authors) (2018) Mega-blowouts in Qinghai–Tibet Plateau: morphology, distribution and initiation. Earth Surface Processes and Landforms. ISSN 0197-9337

https://doi.org/10.1002/esp.4507

Mega-blowouts in Qinghai-Tibet Plateau: morphology, distribution and initiation

Wanyin Luo*[1,2], Zhongyuan Wang[1,3], Junfeng Lu[1], Linghai Yang[1], Guangqiang Qian[1], Zhibao Dong[1,4], Mark D. Bateman[2]

[1] Key Laboratory of Desert and Desertification, Northwest Institute of Eco-Environment and Resources, Chinese Academy of Sciences, Lanzhou, China.

[2.] Geography Department, Sheffield University, Winter Street, Sheffield S10 2TN, UK.

[3] State Key Laboratory of Earth Surface Processes and Resource Ecology, Beijing Normal University, Beijing 100875, China.

[4] School of Geography and Tourism, Shaanxi Normal University, Xi'an, China.

*Corresponding author:

Wanyin Luo, Northwest Institute of Eco-Environment and Resources, Chinese Academy of Sciences, No. 320, West Donggang Road, Lanzhou, Gansu Province 730000, China.

E-mail: wyluo@lzb.ac.cn Tel.: +86-(0)931-496-7498

Abstract：Blowouts are wind-eroded landforms that are widely distributed in the north-eastern part in Qinghai-Tibet Plateau (QTP), China. These blowouts are thought to form in response climate change and/or human activity but little is known about their morphodynamics. Using field surveys, remote sensing and GIS spatial analysis, the distribution and morphology of blowouts are analysed and their initiation considered. Results show the QTP mega-blowouts are some of the largest in the world. The orientations of the trough shaped blowouts are parallel with the prevailing wind, but the saucer and bowl-shaped blowouts are influenced by bi-directional transport. Whilst regional patterns of blowout shape and size were observed to reflect the extent of aeolian sediments and wind regimes, the relationship between the different morphological parameters showed consistency. During initial stages of development, the length-width ratios of blowouts increase rapidly with area but after they reach a mega size this relationship stabilizes as blowouts widen. Initial luminescence dating shows that blowouts appear to have initiated ~100 to 500 years ago, coinciding with the Little Ice Age (LIA) climate event when northwest winds are known to have intensified. Further work is required to confirm this initiation period and establish the significance of mega blowouts for landscape degradation and human activities.

Key words: QTP, mega-blowouts, topography, evolution, age

1. Introduction

Blowouts form due to aeolian deflation of sand from dunes. Deflation forms concave bowl or saucer shaped hollows and down-wind sand is redeposited as an apron (Hesp and Hyde, 1996; Hesp, 2002). Blowout depressions in dunes are found across all latitudes, in arid and semi-arid sandy grasslands and coastal zones (Hugenholtz and Wolfe, 2006). The morphology of blowout depressions are variously described as sand patches, shallow saucers, bowls, or troughs, reflecting the different stages of their development (Hesp, 2002; Hesp et al, 2016). Most blowout depressions are less than 15 metres deep (Hugenholtz and Wolfe, 2006, 2009; Hesp et al., 2016). However, our recent field surveys have revealed that the mega-blowouts at the north-eastern margin of the Qinghai-Tibet Plateau (QTP) are much larger, exceeding 40 m deep and up to 1000 m long. Systematic studies of the present day spatial distribution, morphology and history of these blowouts are needed to determine how and why these types of massive deflation landforms are developing in QTP.

Previous investigations of blowout dunes have focused on the role of aerodynamics (Fraser et al., 1998), wind regime (Jungerius et al., 1991; Hesp et al., 2016) sedimentary structure (Villanueva et al., 2011), and are mainly restricted to coastal dunes (Jungerius et al., 1989; Smyth et al., 2012; Hesp and Pringle, 2001). Once formed, it is thought that blowout growth is limited by negative feedbacks between topography and airflow (Livingstone and Warren,

1996). Long term field monitoring indicates that blowouts reach a critical point in their evolution when wind erosion drops to very low levels at the bottom of the erosion pan (Hugenholtz and Wolfe, 2006). Some geomorphologists have speculated that their formation is typically linked to the reactivation of fixed dunes, the creation of blowouts is therefore seen as a geomorphological response to climate change or a response to land degradation and overgrazing (Hugenholtz and Wolfe, 2006, 2009; Zhang et al., 2006; Hesp et al., 2016). As they develop, blowouts have a positive feedback which causes further reduction of vegetation (land degradation). They may also cause the release of dust into the atmosphere which has a detrimental effect on air quality (Dong et al., 2017). Based on ensemble models, the IPCC (2013) predicts that most arid and semi-arid areas on Earth will become drier over the next century. Of particular concern is the fact that dune reactivation may occur over far shorter (decadal vs millennial) time scales than dune stabilization (Thomas et al., 2005; Hugenholtz and Wolfe, 2005; Barchyn and Hugenholtz, 2012). However, the scarcity of detailed investigations into blowouts means that much remains unknown, especially at the regional scale and in inland settings.

Blowouts are widely distributed across China, including the Mu Us desert, Otindag, Horqin and Hulunber sandy lands (Zhang et al., 2006). Previous studies have investigated blowout pattern classification and development (Zhang et al., 2006), form-flow interaction (Li et al., 2012) and vegetation succession (Zhang et al., 2008). These show that the blowouts in the

grassland areas are mainly formed by the combination of arid climate and the interference of high intensity human activities. The Gonghe Basin in the Qinghai-Tibet Plateau (QTP, Figure 1) is located in the cross section of the westerly wind and Asia and India monsoon. This is an important part of China's desert-loess boundary belt. The unique geographical location and fragile ecosystem make it extremely sensitive to global change, and a key area to study the effects of climate and environmental change on the plateau's environment and surface processes (Yao and Zhu, 2006). Despite the potential importance of these changes, understanding of their regional effect in China is limited by a lack of detailed field studies on the aeolian dune systems in remote areas such as the QTP. Some palaeoclimatological work has been carried out in the Gonghe Basin within the QTP (Dong et al., 1993) which showed that the earliest aeolian sediments in the basin were deposited in the Late Pleistocene episodically between 33.5 to 5.5 ka and since 0.78 ka from present when the climate was colder and drier than today (Qiang et al., 2016; Liu et al., 2013). However, these studies are mostly confined to single areas, and do not compare morphology and distribution between multiple regions. There is also a lack of analysis on varied controlling factors on the morphological evolution process. In this paper, we describe and analyse the distribution and geomorphology of blowouts at a number of different areas across the northeastern part of QTP. This, in combination with their age, are discussed in terms of their evolution of development.

2. Research area and methods

The study was conducted in the northeast edge of the Qinghai-Tibet Plateau (QTP)，an area containing the headwaters of two major river systems, the Yellow River and Yangzi River (Figure 1). The region covers around 30.25×10^4 km^2 has a complex topography (mountains, lakes, desert, steppe and river systems) and diverse vegetation types reflecting the fact that it is the transitional zone between the westerlies and monsoon climate regimes. The region has a cold arid to semiarid continental climate with an average precipitation of (250~400 mm), mean annual temperature ranging from -0.37~3.7℃ and potential evaporation of 1717 mm (Li et al., 2010). Strong north and northwest winds prevail in spring and winter with a maximum wind speed in spring up to 40 m s^{-1} (Li et al., 2010; Dong et al., 1993; Dong et, al., 2017). The region has an average altitude of ~3000 m, glaciers and discontinuous permafrost exists on mountains (Luo et al., 2014; Ran et al., 2018). The global significance of the region for understanding continental geodynamics is widely recognized due to the rich geologic records exposed in the mountain and river systems (Qiang et al., 2016; Dong et al., 2017).

Large areas of aeolian sand are characterized by dune fields and degraded lands that have developed in several dry basins including the Gonghe Basin and the Zoige Basin and in the source regions of the Yellow river valleys

(Maduo) in the northeast edge of the QTP (Figure 1). The combination of a dry, cold, and windy climate with low vegetative cover contributes to wind erosion and leads to the formation of various aeolian landforms. High aeolian transport capacity combined with vulnerable land surface conditions promote various types of blowouts. These are widely distributed in this region (Figure 1), providing a good potential to understand blowout morphodynamics.

2.2 Methods

2.2.1 Morphology parameters extraction

Blowouts were initially identified using high resolution satellite imagery (Worldview in 2008) with a resolution of 0.5 m x 0.5 m. From these images both the edge and the shape of the blowouts were identified and extracted manually. However, due to the limitations of the image resolution, some sand patches and small sized blowouts were not easily recognised even though they were observed in field surveys (e.g. source region of Yangzi River and Shule River). Nevertheless, 2872 individual blowouts were identified from three areas (2625 blowouts from the Gonghe Basin, 169 from the Zoige Basin, and 78 from the Maduo; Table 1) using this approach. Once identified, the area, orientation and length to width ratio for each blowout were measured. Blowouts and their associated depositional lobes were defined on the image on the basis of a combination of clearly visible top of blowout cliff edges and vegetational differences between the bare-sand of blowouts/lobes and

surrounding unbroken vegetated original surfaces. For each feature a shapefile was created using the ArcGIS 10.0 software. Then the field calculator tool was used to calculate the length and width of blowouts and the Linear Directional Mean of Spatial Statistics function to calculate the orientation of blowout. Length was taken as the biggest distance within the shape file from the blowout head to the downwind margin and width as the biggest distance perpendicular to the length. Generally speaking, the blowouts' upwind margin (headwall) was very clear, nevertheless, some sections of margin at the downwind were difficult to define due to the cover of drift sand, especially for those mega-blowouts. In this condition, we determined the downwind margin of blowouts on the basis of visible erosion remnants.

The resultant datasets were then analysed for each area. The remotely derived data was ground truthed in the field to establish whether it had correctly identified the presence of blowouts (as opposed to other geomorphic features). Given the lapse of time between the latest available image (2008) and ground truthing (2015), the latter was not used to verify blowout shape, size or how they were classified. The results shown in this manuscript should therefore represent a true analysis of the blowouts distribution and morphologies as they were in 2008

In aeolian research, it is common to adopt morphological parameters to derive the nature of the force forming geomorphological features and to allow prediction of morphological evolutionary trends (Dong et al., 2012). We

adopted descriptive statistics of the blowouts deflation area (A) and deposition lobe area (S), orientation (θ), length to width ratio (l/w) as base geomorphologic characteristics of the individual blowout (Figure 2d). Previous researchers have classified coastal blowout dunes on the basis of shape (Hesp, 2002; Hesp et al., 2016). Given the order of magnitude changes in size observed in the continental and high altitude QTP blowouts an additional parameter of size has been added to the classification system used here. Adding this additional parameter better characterises the blowouts allowing a more precise defining of the different range of types of blowout. As a result the defined categories are: sand patches (irregular shape, A ≤100 m^2), small blowouts (saucer and bowl blowouts, 100 m^2≤ A ≤ 1000 m^2), medium blowouts (trough blowouts, 1000 m^2 ≤ A ≤ 10000 m^2), mega-blowouts (trough and compound blowouts, A ≥10000 m^2) (Table 1).

Our field survey results also show that blowouts in the source regions of Yangzi, Shule and Datong River are typically small-sized or sand patches. It is difficult extract their morphological parameters through satellite images due to the lack of high resolution imagery in these regions. Furthermore, the blowout populations in these two regions are also much smaller than the other three regions. Consequently, we focussed on regions 3-5 for more detailed descriptions.

2.2.2 OSL dating and age determination

Luminescence dating was conducted on sediments deposited in the sandy aprons deposited next to blowouts. As this technique gives burial ages, samples were selected in an attempt to date the earliest sand eroded from the blowout and deposited within the associated aprons. Such an approach was successfully used by Käyhkö et al. (1999) and Käyhkö (2007) to date the historical development of aeolian landforms during the Holocene in Lapland, Fennoscandia.

Seven samples for luminescence dating were collected from three different blowouts (representing medium and mega-size blowouts) from Gonghe and Mauo area (Figure 3). Three samples (MD1-400, GH1A-250, GH2A-450, indicated as Dep. Lobe in Table 2) were collected from the base of a deposition lobe just above the buried original surface soil using an AMS Regular Soil Auger Kit (3 1/4"). The buried original surface was clearly identifiable on the basis of increase sediment consolidation and a colour change from brown (7.5YR 4/2) to pale brown (10YR 6/3). Three additional samples were taken from the original surface (MD01, GH1-30, GH2A-480, indicated as Original in table 2). These were collected from the same three blowouts as sampled for the depositional lobe but taken from the blowout side wall. According to the deposition lobe development process, the lobe should be thinner and become younger with distance from the blowout. To verify, one additional sample (GH2B-250), was collected from just above the buried original surface soil, 10 metres downwind on the same blowout as sample

GH2A-450Detailed sample information is shown in Table 2 and Figure 3.

Sample preparation was carried out in a darkroom with subdued red light at the luminescence dating laboratory of Key Laboratory of Desert and Desertification, Northwest Institute of Eco-environment and Resources, Chinese Academy of Sciences. All raw samples were treated with 10% HCl and 20% H_2O_2 to remove carbonate and organic matter. The samples were then sieved in water to select grains with the specific sizes of 90–150 μm. Heavy liquid with a density of 2.58 g/cm^3 was then used to extract feldspar fractions. Feldspar grains were treated with 10% HF for 40 min to remove the outer layer, which was irradiated by alpha particles. Then, all samples were treated with 1 mol/L HCl for 10 min to remove fluorides created during the HF etching (Zhao et al., 2012). In order to calculate the dose rate, the Uranium (U), Thorium (Th) concentrations and Potassium (K) content for all samples were determined by means of Neutron Activation Analysis (NAA) in the China Institute of Atomic Energy at Beijing. All dose rate calculations (for alpha dose rate, external dose rate, internal dose rate, and cosmic dose rate) follow the detailed description in Long et al. (2014) and references therein. Infra-red stimulated luminescence (IRSL) were conducted in a Risø luminescence reader with palaeodoses (De) derived using the single aliquot regeneration (SAR) protocol of Murray and Wintle (2003). Measurements were the single aliquot level (diameter 9.5 mm) with multiple replicates (between 6-12) measured for each sample. Measurements were only accepted for inclusion in

age calculations where they exhibited rapid shine down, good growth curve characteristics and recycling within 10% of unity. Although the number of replicates measured per sample was low, high levels of replicate reproducibility were seen. As a result, we can have high confidence that ages based on mean De values (as calculated from the arithmetic mean) from each samples should be giving us the true sediment burial age (Table 2). Ages are presented in years from measurement (2015) with one sigma confidence limits.

3. Results

3.1 Distribution and morphology

Based on our field survey results and image analysis, blowouts can be found in a range of geomorphic settings from dry basins, wide river valleys, lakeshores and mountain slopes. As shown in Figure 1, blowouts are found at the source region of Yangzi River; Shule and Datong rivers; source regions of Yellow River; Zoige Basin, the low-part source region of the Yellow River and Gonghe Basin, the upper-reaches of Yellow river. But, mainly distributed in Maduo, Zoige and Gonghe Basin.

3.1.1 Maduo

Blowouts in this region are relatively sparse, mainly being distributed around lake shores and river channels in the source area of the Yellow River. The

source of sand material for the blowouts formation in this area is mainly the palaeo-aeolian sediments and modern river alluvium. The average blowout area in this region is 1957 m^2 with only a few medium-sized blowout areas more than 10,000 m^2. The average blowout length to width ratio was 2.2 and varied between 1.5 and 2.5 (Figure 4). Blowout orientations are mainly concentrated between 90° to 115° (Figure 5a), which accounts for 53% of the total blowouts population in this region.

3.1.2 Zoige Basin

In Zoige Basin, the blowouts are mainly distributed in the boggy meadows and the sandy grassland along both sites of the Yellow River. The alluvial sediments and the paleo sand deposits are the main source materials for the blowouts in this area. Sand deposits are limited, as is the size and apparent rate of blowout expansion. As a result, most of the blowouts in this region are small to medium sized, with an average area of 2524 m^2. These varied from 77 m^2 to 22,370 m^2. The average length to width ratio in this region is 1.67, with 80% of blowouts having a ratio smaller than 2. The blowout orientations also show a wide range, mostly oriented in 28°-135° (Figure 5b).

3.1.3 Gonghe Basin

Gonghe Basin is located in the northeast edge of QTP, where blowouts have typically developed on the terraces of the north bank of the Yellow River. The morphology of the blowouts in Gonghe Bbasin are typically saucer, bowl and trough shaped using Cooper (1958) and Hesp's (2002) and Hesp et al.'s (2016)

classifications in coast regions. As shown in Table 1, only a small number of mega-blowouts have an area of more than 10,000 m^2, and most are between 100 m^2-10,000 m^2. The largest mega-blowouts reach 177,000 m^2, and lengths of up to 1000 m (including the deposition lobe). Blowout depths, measured from the bottom of the deflation pan to the top of the erosion wall edges, varied between 8 and 40 m for the medium and mega-sized blowouts, and 0.5 and6 m for the small blowouts, and 0.2 and0.5 m for sand patches. Our analysis also shows that the blowout lengths and widths appear quite strongly correlated (Figure 4). Apart from the sand patches and some small blowouts, the length to width ratio of medium and mega-blowouts range between 2 and 2.5, with an average of 2.47, which covers most of the blowouts in this site. Fewer than 10% of blowouts have a length to width ratio less than 1.5. The length to width ratio of small blowouts is the lowest. In general, the length to width ratio appears to increase between small and medium sized blowouts, but to decline for larger sized blowouts.This suggests that in earlier stages of development, blowouts mainly extend longitudinally. In the middle and late stage of blowout development, lateral abrasion of the side walls and its collapse may be the main expansion processes consistent with other blowouts (Abhar et al., 2015; Hugenholtz and Wolfe, 2006).

The evolution of blowouts, and in particular, their orientation, may be influenced by the variation in regional winds strength and direction (Gares, 1992; Byrne, 1997). Small blowouts show a wide range in orientation (0-180°) ,

whereas medium and mega-sized blowouts in Gonghe area are mainly concentrated between 90° to 160°, agreeing well with the local prevailing wind and drift potential direction (Figure 5c). The narrow-long shape of mega blowouts, generally oriented between 110° to 135° , are probably due to development over a long period with under relatively, stable unidirectional winds. As a secondary effect, it is also noted they occur only where topographic relief is low, minimising air flow disturbance and localised steering.

3.2 Blowout age and potential climate proxy

The size and deflation rate should be related to the initiation age of blowouts, especially for the mega-blowouts in Gonghe Basin which show a downwind expansion trend. Even though at the initiation stage when blowout size is small (sand patches and small blowouts) and depositional lobes poorly defined, elongate blowouts exhibit a form-flow feedback. Large vortices-based flow becomes significant lead to undermining, collapse and retreat of blowout back walls (Hesp, 2002) allowing upwind expansion (Hesp and Hyde, 1996; Jungerius and Meulen 1989). Our field monitoring and observations in the Gonghe Basin also reveal that mega-blowouts are prone to grow lengthwise against the prevailing NW wind (Figure 6). This means that once a blowout forms, the downwind edge rapidly becomes buried under the depositional apron and is therefore more stable than the blowout sides and up-wind head walls. Therefore, the sediment above the buried original surface soil horizons

just in the upwind edge of the deposition lobe can be used to represent the initial age of the blowouts (Clarke and Käyhkö, 1997; Sawakuchi et al., 2008).

Drilling at the sampled site showed that overlying the older original surfaces the depositional lobe was 3.0 m thick for B1 and 4.6 m thick for B2 in Gonghe area and 4.4 m for Maduo area. The four aeolian samples from the base of the depositional lobe yielded age estimates of 0.14±0.03ka (GH1A-250), 0.5±0.03ka (GH2A-450), 0.31±0.06ka (GH2B-250) and 0.09±0.02ka (MD1-400). A these have not been corrected for any potential anomalous fading, initiation may have occurred a little before this time. However, with only four ages which show high levels of inter-site age variability, more ages are required to to better establish the timing of blowout initiation. In contrast, the stratigraphically lower original surface soil samples yielded ages of 1.16±0.06ka (GH1-30), 2.22±0.05ka GH2A-480 and 0.34±0.03ka (MD01), respectively. The ages from sediments overlying the original surface in each sampling site are, as would be expected, much younger than those beneath the original surface.

The dating results indicate that the age of mega-blowouts vary, with the oldest (B2) in Gonghe Basin dating to ~500 years and the youngest blowout in Maduo area dating to ~90 years (Table2). In contrast, the pre-existing sediments before blowout initiation are around 300-2,200 years old. Also, a noticeable dating result is that the age of 0.31±0.06ka (GH2B-250) further downwind on the depositional lobe is younger than 0.5±0.03ka (GH2A-450).

Both of these age sequences therefore confirm our idea of stratigraphy and dating hypothesis.

It would appear that initial formation of blowouts in the QTP may have coincided with the Little Ice Age (LIA) as indicated by the ice core dust record in the ice cap records from around this region (Yao et al., 1990; Yang et al., 2006). The LIA in this region of the world is thought to have started in the 1400s and extended to the 1700s (Yao et al., 1990; Yang et al., 2006). According to the Dunde ice core (only 400 km away from the northeast of Gonghe Basin), dust content shows a linear trend increasing over the past 700 years with high dust amounts during the LIA cold period indicating strong intensified northwest winds (Yang et al., 2006). Tree ring and lacustrine sediments records near the research area have also been used to construct a drought history for the past 500 years (Yang et al., 2014; Liu et al., 2016; Qiang et al., 2013). Of particular note, Liu et al. (2013) reported a prominent cold and dry stage from 700 years ago associated with increased aeolian activity in the Gonghe Basin. Additionally, Qiang et al. (2013) recovered a high-resolution Holocene record of aeolian activity from the sediments of Genggahai Lake in the Gonghe Basin by assuming that the lake sediment's sand fraction was transported into the lake primarily by strong winds. The period of most intense aeolian activity occurred from 200 to 100 years BP.

4. Discussion

4.1 Morphological parameters and their dynamical meaning

In aeolian geomorphology research, relations between morphometric data (spacing, length, height and defect density) have morphological significance (Ewing et al., 2006; Ewing and Kocurek, 2010). These parameters tend to change as a function of time. In this paper, we use the characteristic morphological parameters to assess the morphological evolution of blowouts.

As Figure 9 shows, the cumulative frequency curve of the blowout areas is smooth with a similar trend to desert dunes (Ewing and Kocurek, 2010) suggesting that blowouts have similar self-organizing rules as aeolian accumulative landforms (Kocurek and Ewing, 2005). From our data it would appear that medium and large-sized blowouts are generally aligned from NW-SE or WNW-ESE (77% of those measured in these size categories). This indicates that as blowouts develop and mature the orientations become more concentrated and stable at a regional level. This evolution is also consistent with the trend of desert sand dunes observed by Ewing et al. (2006). The reasons for this phenomenon are mainly due to small blowouts' unstable shape, dramatically influenced by external environmental conditions. However, the shape of medium and large blowouts is stable, producing a uniform trend after prolonged wind erosion. Mega-blowout length to width ratios show the highest values under the prevailing wind direction. This indicates that the effects of higher frequency wind events on blowouts geomorphology are significant. This is in accordance with Jungerius et al.'s (1991) and Jungerius

and Meulen (1989) monitoring results in coastal dune blowouts in Netherlands. They observed the phenomenon that high frequency climate events had the most obvious effect on the evolution of blowouts under different wind regimes.

As essentially a 'closed system', sand released from the deflation basin accumulates downwind in the deposition lobe, except for a small amount of fine dust which can be transported and deposited much further away (Hugenholtz and Wolfe, 2006). Therefore, it could be expected that the area of the deposition lobe should increase as the area of the deflation basin also increases. Our results, however, revealed that the area ratio of the deposition lobe and the deflation basin (S/A) decreased as the area of the blowouts increased (Figure 8). This can be explained by changes to the aeolian transport dynamic process as blowouts develop. In the initial stages, the sand entrained by the wind from the deflation basin form a sheet along the wind direction. As sand is deposited on the deposition lobe the original vegetated surface is buried and replaced by a sand. This reduces the surface roughness, increases the fetch distance of aeolian sand transport and through a positive feedback allows eroded sand to be more easily transport on the depositional lobe and deposited further along it. At this stage, the deposition lobe area of a blowout commonly is far greater than the deflation basin resulting in a large ratio of these two parameters. However, as the size of the blowouts enlarges, the total amount of sand released from the blowout deflation basin increased, promoting sand accretion on the deposition lobe leading to the formation of a

transverse dune (Dong et al., 2007). The topographical effect of the dune changes the carrying capacity of the wind and the mass balance within the blowouts (Hugenholtz and Wolfe, 2006; Hesp et al., 2016). The dunes therefore reduce the distance over which sand is transported limiting the expansion in size of the depositional lobe. As a result, the ratio of the area between the deflation basin and sand deposition lobe is reduced.

4.2 Development processes

Previous researchers have attempted to identify different stages of blowout development (Gares et al., 1995; Hesp, 2002). They suggest that blowouts may evolve in various ways, the pattern depending on wind speeds, dominant wind direction, vegetation types and revegetation processes and potential, magnitude and occurrence of beach/dune erosion and storm events, and barrier/beach status (receding, stable, prograding). Hesp et al. (2016) also found that the Cape Cod beach dune blowout evolution may tend to follow multiple stages, which is quite different to those observed elsewhere.

With such a large dataset encompassing a wide range of blowout sizes and shape, the QTP results also provide some insight into how blowouts expand through time. It is clear that the blowout length to width ratios increase with area as blowout size increases from small to medium before reaching a plateau for mega-blowouts (Figure 9). This developmental feature is also consistent with the deformation trend described by Livingstone et al. (1996)

and Cooper (1958). In the early stage of development, due to the "narrow tube effect", the high frequency turbulence airflow promotes blowout growth in the long axis so that the length to width ratio also increases. However, the blowouts also widen and deepen with maturity. Side wall collapse supplies more sand, which is entrained by laterally deflected winds outside the blowouts where it can settle on the top of the downwind deposition lobe. This change in deflation basin flow circulation leads to blowouts more oriented with the lateral expansion.

Whilst triggers may vary from area to area within north-eastern QTP, this affects only the earlier stages of blowout formation. Focusing on a single area and only on blowouts found in the high alpine area we propose that the development of inland blowouts passes through the following key stages (Figure 10):

1) **Embryonic stage**

In this stage only sand patches take place ($A<100m^2$, length to width ratio around 1), with disparate orientations and are recognized as the embryonic stage of the blowouts. Sand patches are a direct response to the original vegetated surface being disrupted by wind erosion, human and animal activities. With a disrupted surface, the underlying aeolian sand becomes subjected to erosion.

2) **Initial stages**

Through the deepening and expansion of the deflationary area reduced surface friction enhancing the erodibility of underlying sand causing sand patches to deepen and expanded to generate saucer and bowl-shaped small blowouts ($100m^2<A<1000m^2$, length to width ratio 1-2). In this initial stage, the blowouts are immature and have no obvious stable morphological features and deposition lobes.

3) **Adolescent stage**

With the undergo further deepening and expansion saucer and bowl blowouts will extend rapidly both in lateral and vertical direction, some small blowouts are merged together to form medium-sized trough blowouts ($1000m^2<A<10000m^2$, length to width ratio 2.0-3.0). In this stage, the blowout side wall and head wall getting steeper and a downwind narrow long deposition lobe along the prevailing wind always being visible. Blowout's marginal growth in this stage always rapidly according to our field monitoring.

4) **Mature stage**

Localised high velocity and turbulent airflow in the deep deflation pan within trough blowout in stage 3 promotes the collapse of the side wall,

inducing complexed form-flow interaction. At this stage some neighbouring medium sized blowouts may continue merging and finally enlarged into a mega sized trough blowout (A>10000m^2, length to width ratio 2.0-5.6). The blowout morphology reaches its prime status with established depositional aprons and with transverse dunes. blowouts in this stage relatively show stable external features, marginal erosion is still more predominant than the vertical deeping.

.

In the coastal regions, many blowouts become larger overtime and may evolve into parabolic dunes (Hesp and Hyde,1996; Hesp, 2002). Blowouts can also advance through evolutionary stages from erosional notches, to incipient blowouts, to large blowouts, to decaying and revegetating blowouts (Gares and Nordstrom, 1995). In the QTP, however, no obvious parabolic dunes were found during our field survey and monitoring. This may be due to the lack of shrubs and low grass growth rates due to the low temperatures and high altitude limiting sand capture once the depositional lobes start to spread downwind on to grass land.

5. Conclusions

This work documents extensive blowouts in QTP, some of which are of a mega-size. It also shows that regional differences exist in both the morphology of the blowouts and in the controlly factors that create them. The development

of the QTP blowouts can be divided into four stages (embryonic, initial, adolescent，mature), representing different levels of maturity. The blowout morphological parameters reflect a strong relationship both with wind direction and recent climate changes which have caused surface disturbance of vegetation and sediments. Initial dating results reveal that blowouts formed 100 to 500 years ago, coinciding with the Little Ice Age when winds are thought to have been more intense and a drought is known to have occurred. Further research using continued field morphological monitoring and detailed dating work at the regional scale is required to better understand both the initiation mechanisms and the relationships between blowouts, climate change and human activities.

Acknowledgments

This work was funded by the National Natural Science Foundation of China (41371026; 41771015) and Key Project from the Ministry of Science and Technology of the People's Republic of China (2013CB956003). Professor Zhao and Miss Peng are appreciated for luminescence sample preparing and measurements. We are also grateful to Dr Jichun Wu for the discussion on the research proposal and provide some useful suggestions. Wanyin Luo acknowledges the wonderful support from the China Scholarship Council and the University of Sheffield for hosting him be an academic visitor. The three

anonymous reviewers and Dr Robert Bryant (University of Sheffield) who read and provided detailed constructive comments on this manuscript are also thanked.

References:

Abhar KC, Walker IJ, Hesp PA, Gares PA. 2015. Spatial–temporal evolution of aeolian blowout dunes at Cape Cod. Geomorphology 236:148-162

Barchyn TE, Hugenholtz CH. 2012. Predicting vegetation-stabilized dune field morphology. Geophysical Research Letters, 39: 61-65.

Byrne ML. 1997. Seasonal sand transport through a trough blowout at Pinery Provincial Park, Ontario. Canadian Journal of Earth Sciences 34: 1460–1466.

Clarke ML, Käyhkö JA. 1997. Evidence of Holocene aeolian activity in sand dunes from Lapland. Quaternary Science Reviews 16: 341-348.

Cooper WS. 1958. Coastal Sand Dunes of Oregon and Washington. The Geological Society of AmericaMemoir,72. Waverly Press :Baltimor.

Dong GR, Gao SY, Jin J. 1993. Aeolian Desertification and its Control in Gonghe Basin of Qinghai Province (in Chinese with English summary). Science Press: Beijing.

Dong ZB, Qian GQ, Luo WY, Wang HT. 2007. A wind tunnel simulation of the effects of stoss slope on the lee airflow pattern over a two-dimensional

transverse dune. Journal of Geophysical Research: Earth Surface 112, , DOI:10.1029/2006JF000686.

Dong ZB, Lv Ping, Lu Junfeng, Qian Guangqiang, Zhang Zhengcai, Wanyin Luo. 2012. Geomorphology and origin of Yardangs in the Kumtagh Desert, Northwest China. Geomorphology 139-140: 145-154.

Dong, ZB., Hu, GY., Qian, GQ., Lu, JF., Zhang, ZC., Luo, WY., & Lyu, P. 2017. High-altitude Aeolian research on the Tibetan Plateau. Reviews of Geophysics, 55:1-38. doi.org/10.1002/ 2017RG000585.

Ewing RC, Kocurek G, Lake LW. 2006. Pattern analysis of dune-field parameters. Earth Surface Processes and Landforms 31: 1176-1191.

Ewing RC, Kocurek G. 2010. Aeolian dune-field pattern boundary conditions. Geomorphology 114: 175-187.

Fraser GS, Bennet SW, Olyphant GA, et al. 1998. Windflow circulation patterns in a coastal dune blowout, south coast of Lake Michigan. Journal of Coastal Research 14: 451–460.

Gares PA, Nordstrom KF. 1995. A cyclic model of foredune blowout evolution for a leeward coast: Island Beach, New Jersey. Annals of the Association of American Geographers 85: 1– 20.

Gares PA. 1992. Topographic changes associated with coastal dune blowouts at island beach State Park, New Jersey. Earth Surface Processes and Landforms 17: 589–604.

Hesp P. 2002. Foredunes and blowouts: initiation, geomorphology and dynamics. Geomorphology 48: 245-268.

Hesp PA, Hyde R. 1996. Flow dynamics and geomorphology of a trough blowout. Sedimentology 43: 505-525.

Hesp PA, Pringle A. 2001.Wind Flow and Topographic Steering within a Trough Blowout. Journal of Coastal Research （Special 34): 597-601.

Hesp PA, Smyth TAG, Walker IJ, Gares PA, Wasklewisz. 2016. Flow within a Trough Blowout at Cape Cod. Journal of Coastal Research (SI 75): 288-292

Hugenholtz CH, Wolfe SA. 2005. Biogeomorphic model of dunefield activation and stabilization on the northern Great Plains. Geomorphology 70: 53-70.

Hugenholtz CH, Wolfe SA. 2006. Morphodynamics and climate controls of two aeolian blowouts on the northern Great Plains, Canada. Earth Surface Processes and Landforms 31(12): 1540-1557.

Hugenholtz CH, Wolfe SA. 2009. Form–flow interactions of an aeolian saucer blowout [J]. Earth Surface Processes and Landforms, 34: 919-928.

Stocker TF, et al. 2014. Climate change 2013: the physical science basis. Contribution of Working Group I to the Fifth Assessment Report of IPCC the Intergovernmental Panel on Climate Change. Cambridge University Press: Cambridge.

Jungerius PD, Meulen FVD. 1989. The development of dune blowouts, as measured with erosion pins and sequential air photos. Catena 16(4-5): 369-376.

Jungerius PD, Witter JV, van Boxel JH. 1991. The effects of changing wind regimes on the development of blowouts in the coastal dunes of The Netherlands. Landscape Ecology 6(1-2):41-48.

Käyhkö JA, Worsley P, Pye K, Clarke ML. 1999. A revised chronology for aeolian activity in subarctic Fennoscandia during the Holocene. The Holocene 9(2):195–205.

Käyhkö JA. Aeolian blowout dynamics in subarctic Lapland based on decadal levelling investigations. Geografiska Annaler, 2007, 89(1):65-81.

Kocurek G, Ewing RC. 2005. Aeolian dune field self-organization – implications for the formation of simple versus complex dune-field patterns. Geomorphology 72: 94-105.

Li S, Yang P, Dong YX,et al. 2010. Wind-driven Land Degradation and its Control in Xizang (Tibet) (in Chinese). Science Press: Beijing.

Li SQ, Hasi ED, Du HS,et al. 2012. Interaction between Airflow and Shape of Saucer Blowout in Sandy Grassland. Journal of Desert Research 32(5):1201-1209.

Liu B, Jin HL, Sun LY, Su ZZ, Zhang CX, Zhao S. 2016. History of moisture change derived from slope sediments of the eastern Gonghe Basin (northeastern Qinghai–Tibetan Plateau) during the last 17ka. Geological Journal. DOI: 10.1002/gj.2795

Liu, B, Jin, HL. Sun LY, Sun Z, et al. 2013. Holocene climatic change revealed by aeolian deposits from the Gonghe Basin, northeastern Qinghai-Tibetan Plateau. Quat. Inter. 296, 231-240.

Liu B, Jin HL. Sun LY, Sun Z, et al. 2013. Holocene climatic change revealed by aeolian deposits from the Gonghe Basin, northeastern Qinghai-Tibetan Plateau. Quaternary. International 296: 231-240.

Livingstone I, Warren A.1996. Aeolian Geomorphology: An Introduction, Longman Singapore Publishers (Pte) Ltd: London

Long H, Shen, J, Tsukamoto S, Chen J, Yang L, Frechen M. 2014. Dry early Holocene revealed by sand dune accumulation chronology in Bayanbulak Basin (Xinjiang, NW China). Holocene 24: 614-626.

Luo DL, Jin HJ, Sergei M, Vladimir R. 2014. Distribution and changes of active layer thickness (ALT) and soil temperature (TTOP) in the source area of the Yellow River using the GIPL model. Science China Earth Sciences 57: 1834–1845.

Murray AS, Wintle AG. 2003. The single aliquot regenerative dose protocol: potential for improvements in reliability. Radiation Measurements. 37: 377–381.

Qiang MR, Chen FH, Song L, et al. 2013. Late Quaternary aeolian activity in Gonghe Basin, northeastern Qinghai-Tibetan Plateau, China. Quaternary Research 79: 403-412.

Qiang MR, Jin YX, Liu XX, Song L, Li H, Li FS, Chen FH. 2016. Late Pleistocene and Holocene aeolian sedimentation in Gonghe Basin, northeastern Qinghai-Tibetan Plateau: Variability, processes, and climatic implications. Quaternary Science Reviews 132: 57-73.

Ran YH, Li X, Cheng GD. 2018. Climate warming over the past half century has led to thermal degradation of permafrost on the Qinghai–Tibet Plateau. The Cryosphere 12: 595–608.

Sawakuchi AO, Kalchgruber R, Giannini PCF Nascimento Jr DR, Guedes CCF, Umisedo NK. 2008. The development of blowouts and foredunes in the Ilha Comprida barrier (Southeastern Brazil): the influence of Late Holocene climate changes on coastal sedimentation. Quaternary Science Reviews 27: 2076–2090.

Smyth TAG, Jackson DWT, Cooper JAG. 2012. High resolution measured and modelled three-dimensional airflow over a coastal bowl blowout. Geomorphology 177-178: 62-73.

Thomas DSG, Knight M, and Wiggs GSF. 2005. Remobilization of southern African desert dune systems by twenty-first century global warming. Nature 435: 1218–1221.

Villanueva RG, Costas S, Duarte H, et al. 2011. Blowout evolution in a coastal dune: Using GPR, aerial imagery and core records. Journal of Coastal Research 64: 278-282.

Yang B, Qin C, Wang JL, He MH, Melvin TM, Osborn TJ, Briffa KR. 2014. A 3,500- year tree-ring record of annual precipitation on the northeastern Tibetan Plateau. Proceeding of the National Academy of Sciences of the United States of America111: 2903–2908.

Yang MX, Yao TD, Wang HJ. 2006. Microparticle content records of the Dunde ice core and dust storms in northwestern China. Journal of Asian Earth Sciences 27: 223–229.

Yao TD, Xie ZC, Wu XL,Thompson LG. 1990. Little ice age recorded by Dunde ice Cap. Science inChina 11B, 1196–1201.

Yao TD, Zhu LP. 2006. The response of environmental changes on Tibetan Plateau to global changes and adaptation strategy (in Chinese with English abstract). Advances in Earth Science 21: 459–464.

Zhang DP, Wang XK, Hasi ED, Sun HW, Zhao JM, Liu X, Feng Zongwei 2006.HulunBuir Sandy Grassland Blowouts: Geomorphology, Classification and Significances (in Chinese with English abstract). Journal of Desert Research 26: 894-902.

Zhang P, Hasi ED, Wang S, Zhang SH. 2008. Zonation of Vegetation on Depositional Area of Blowout in Hulun Buir Grassland (in Chinese with English abstract). Journal of Natural Resources 23: 237-244.

Zhao H, Li GQ, Sheng YW., Jin M, Chen FH. 2012. Early-middle Holocene lake-desert evolution in northern Ulan-Buh desert, China. Palaeogeography, Palaeoclimatology, Palaeoecology 331-332: 31-38.

Table 1. Blowouts area of different category in the three research area in QTP

category / sites	Sand patches ($\leq 100m^2$)	Small blowouts ($100\text{-}1000m^2$)	Medium blowouts ($1000m^2\text{-}10000m^2$)	Mega-blowouts ($\geq 10000m^2$)	Total (n)
Gonghe	252	1458	761	154	2625
Zoige	3	85	69	12	169
Maduo	60	15	2	1	78

Table 2 IRSL related data for sampled sites within the blowout deposition lobes. Note samples described as Original relate to sediments into which the blowout was formed so should be older than the blowout itself. Samples described as "Dep. Lobe" were taken at the base of the depositional lobe and should give initiation ages for the associated blowout.

Area/Site	Sample Code	Sample description	Particle size (μm)	Aliquot number (n)	Mean De (Gy)	U (ppm)	Th (ppm)	K (%)	Water content (%)	Total dose rate (Gy/ka)	Age (ka)
Maduo											
1	MD01	Original	90-150	12	0.70±0.06	1.16±0.06	5.44±0.18	0.96±0.04	4.7±1%	2.09±0.10	0.34±0.03
	MD1-400	Dep. Lobe	90-125	12	0.19±0.03	1.22±0.06	5.60±0.17	1.00±0.04	12±1%	2.01±0.10	0.09±0.02
Gonghe											
B1	GH1-30	Original	90-150	12	4.05±0.19	2.09±0.08	10.8±0.28	1.71±0.05	2.3±1%	3.48±0.13	1.16±0.06
	GH1A-250	Dep. Lobe	90-150	12	0.41±0.06	1.42±0.07	7.23±0.21	1.50±0.05	3.7±1%	2.88±0.11	0.14±0.03
B2	GH2A-450	Dep. Lobe	90-150	12	1.34±0.03	1.39±0.07	6.95±0.20	1.59±0.06	9.7±1%	2.71±0.09	0.50±0.03
	GH2A-480	Original	90-150	6	6.29±0.17	1.53±0.06	7.89±0.24	1.70±0.04	12±1%	2.83±0.10	2.22±0.05
	GH2B-250	Dep. Lobe	90-151	6	0.87±0.07	1.35±0.07	6.58±0.21	1.65±0.05	10±1%	2.77±0.17	0.31±0.06

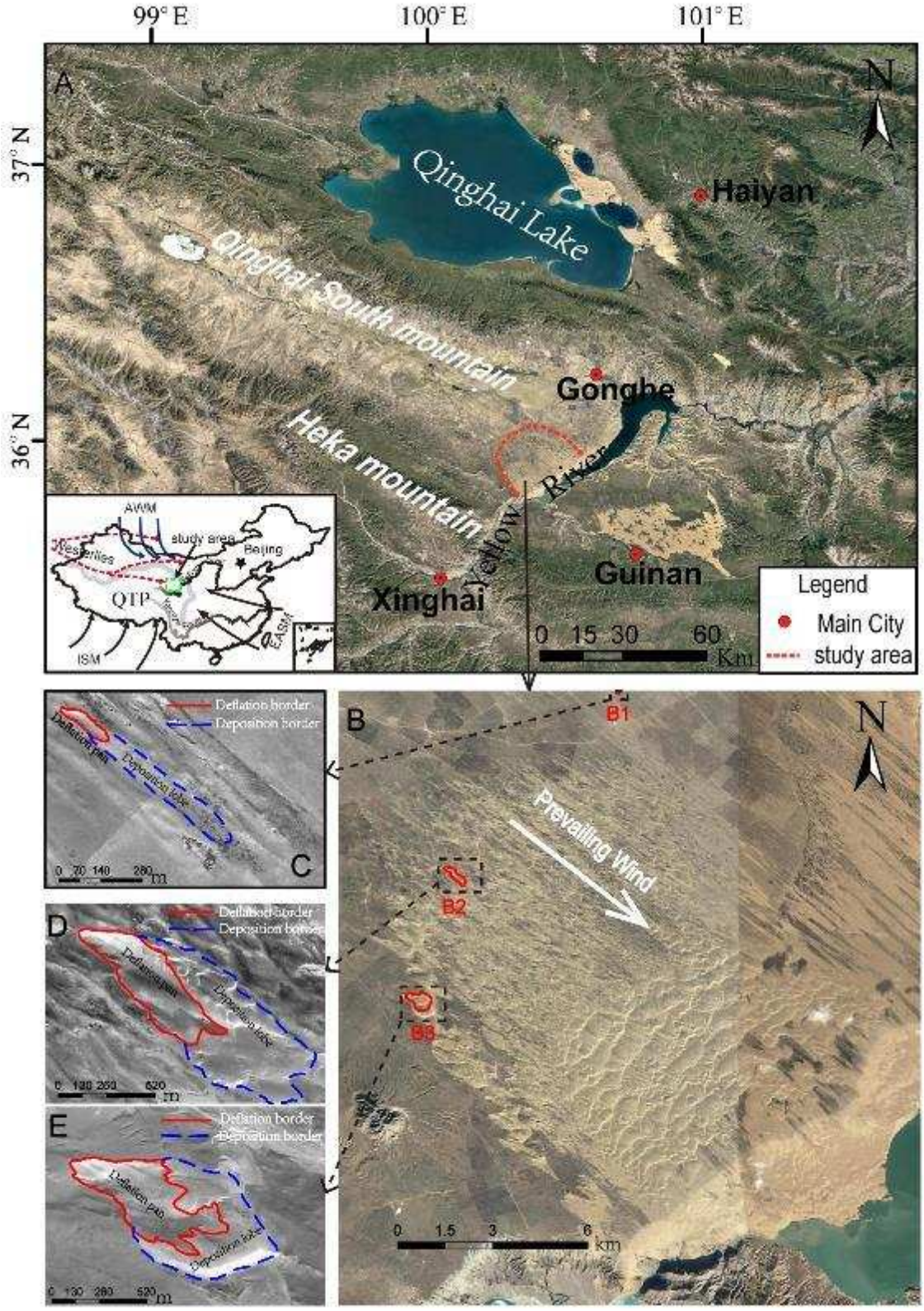

Figure 1. Topographic map of China and typical mega-blowouts in Qinghai-Tibet Plateau (QTP). (A) landscape map of the study area and its major atmospheric systems, AWM= Asian winter monsoon, ISM= Indian summer monsoon, EASM= East Asian summer monsoon; (B) satellite image of the research site, the red polygons represent the three monitoring mega-blowouts. The mega-blowouts are mainly distributed on the upwind edge of the activated dunes. (C-E) high-resolution image of

monitored blowouts (Worldview II, 2008), showing both the size and the border of the deflation basin or plain and the depositional lobe)

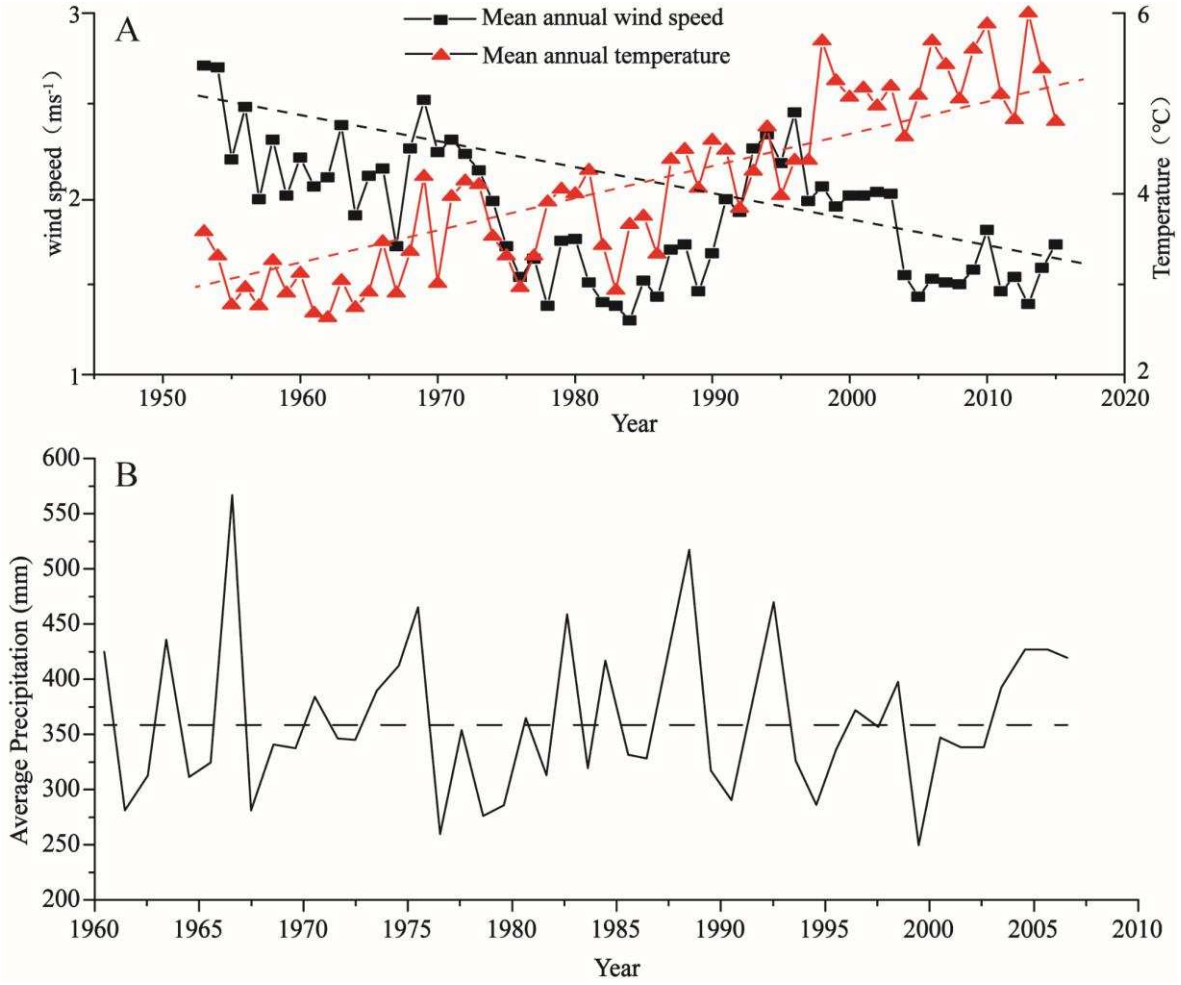

Figure 2 Historic precipitation and wind conditions in the research area in the past 60 years. Data provided by the Meteorological Network, China Meteorological Administration (E100.37°, N36.16°, http://data.cma.cn/)

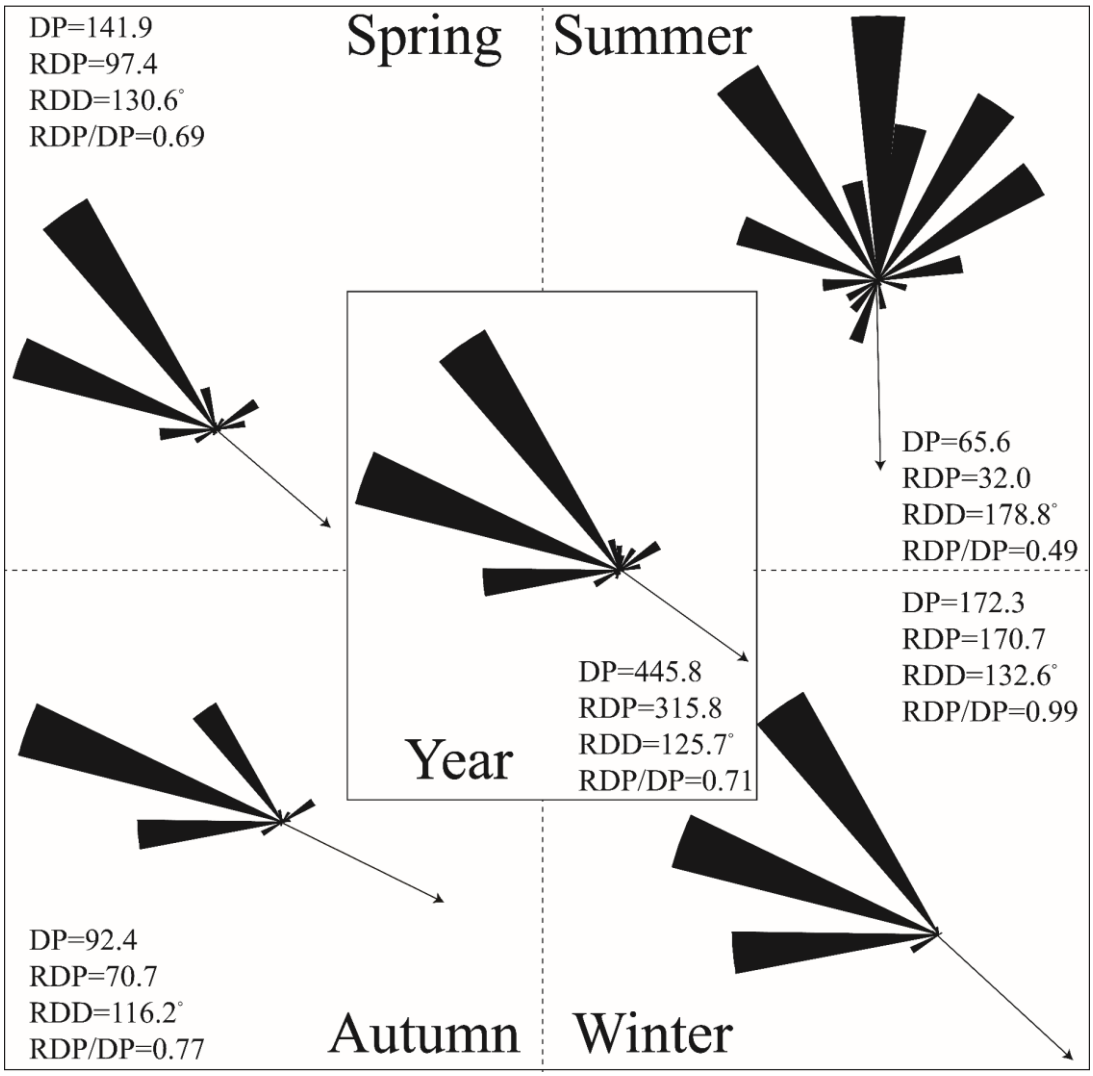

Figure 3 The seasonal and annual sediment transport potential in the study area.

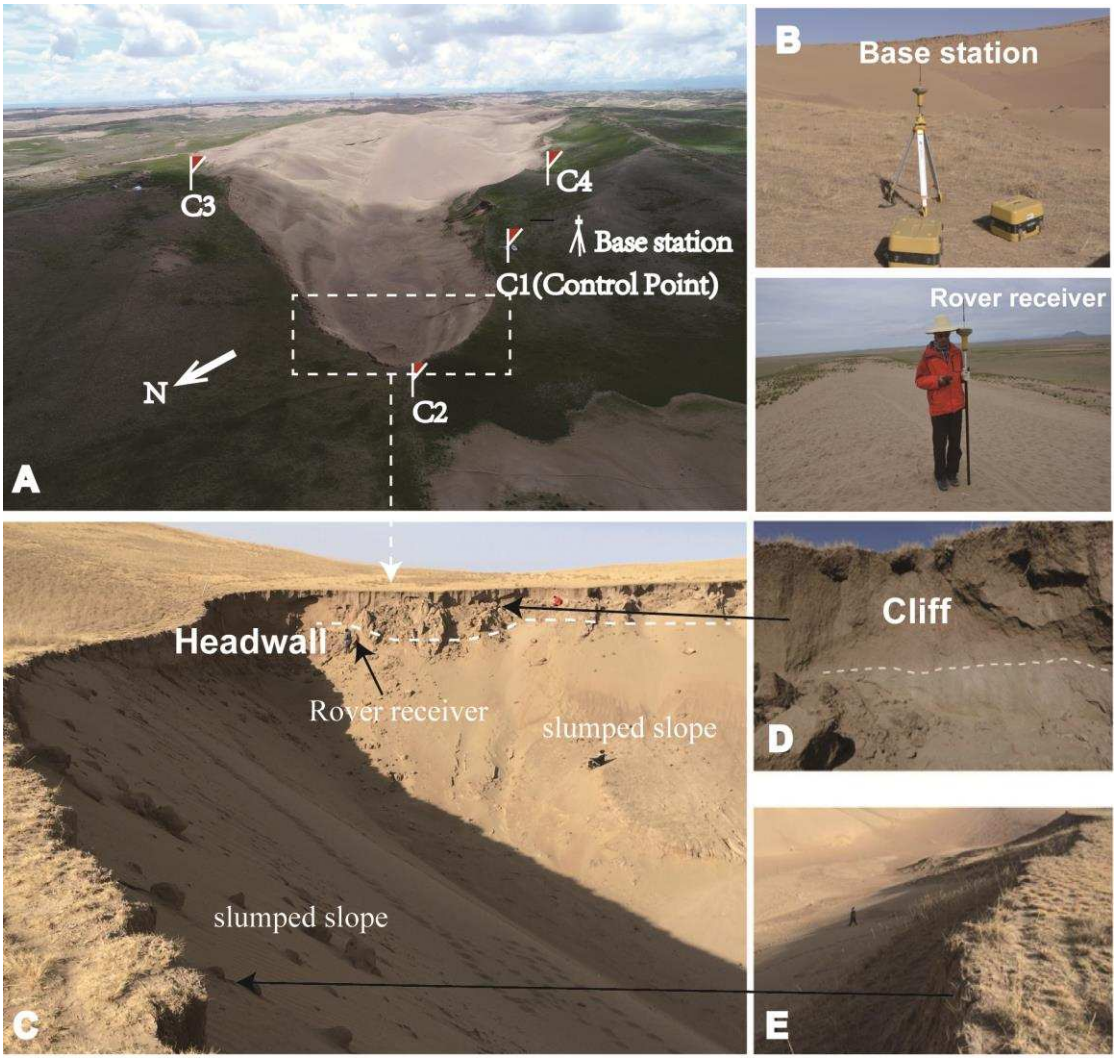

Figure 4. Geomorphology features of Monitoring mega-blowout and the equipment and ground control system A. top view of blowout B3 as well as the measuring control system. Note the house on the left of the C3 flag for scale; B. RTK-GPS base station and rover receiver; C-E. typical features of different part of mega-blowout. Notice the head part depth and the cliff height and massive falling block), and humans (arrowed) for scale.

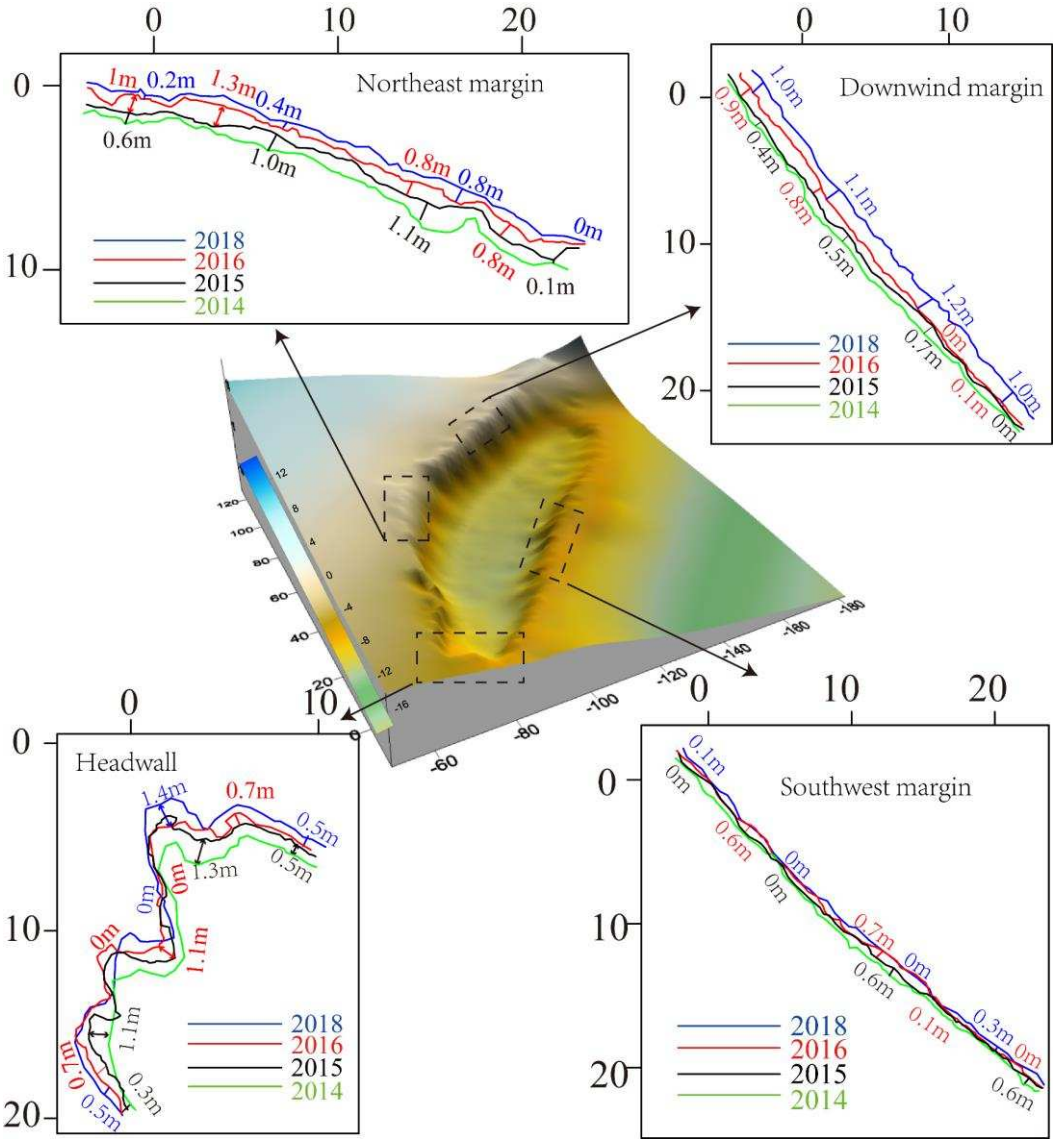

Figure 5 The morphological margin expansion of monitored blowout B1 .

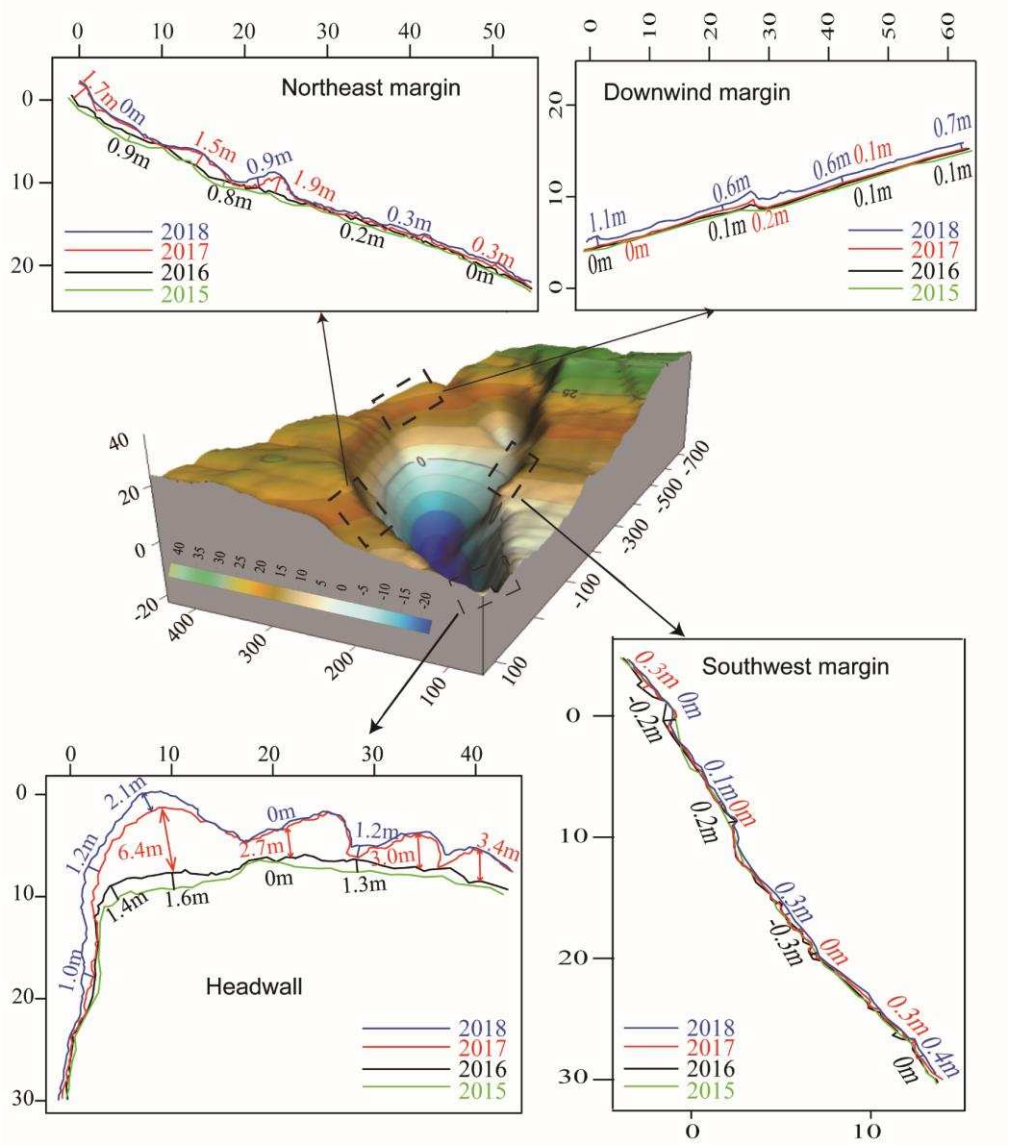

Figure 6 The morphological expansion of monitored blowout B2.

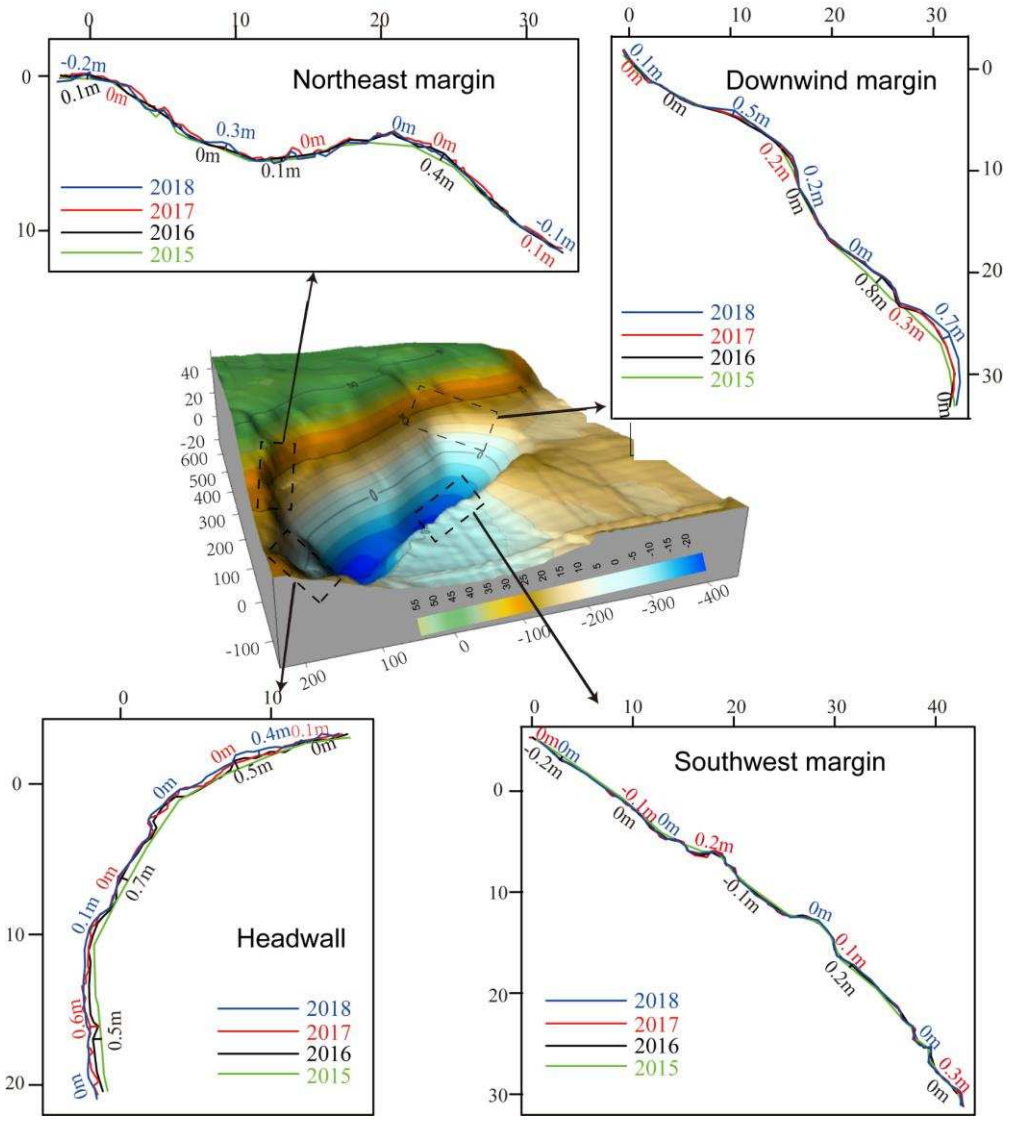

Figure 7 The morphological expansion of monitored mega-blowout B3.

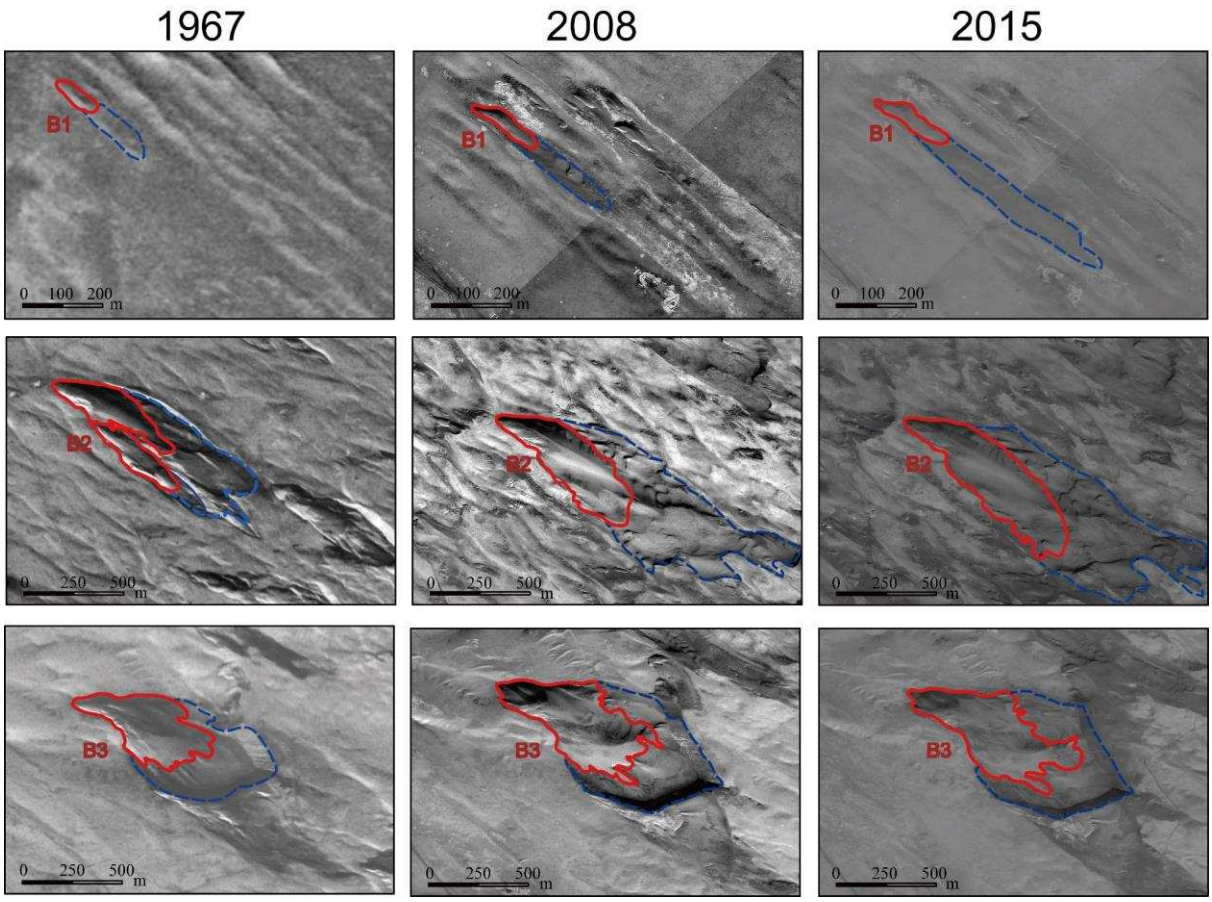

Figure 8 Historical expansion of monitored mega-blowouts from 1967 to 2015. (Aerial image and satellite image comparision)

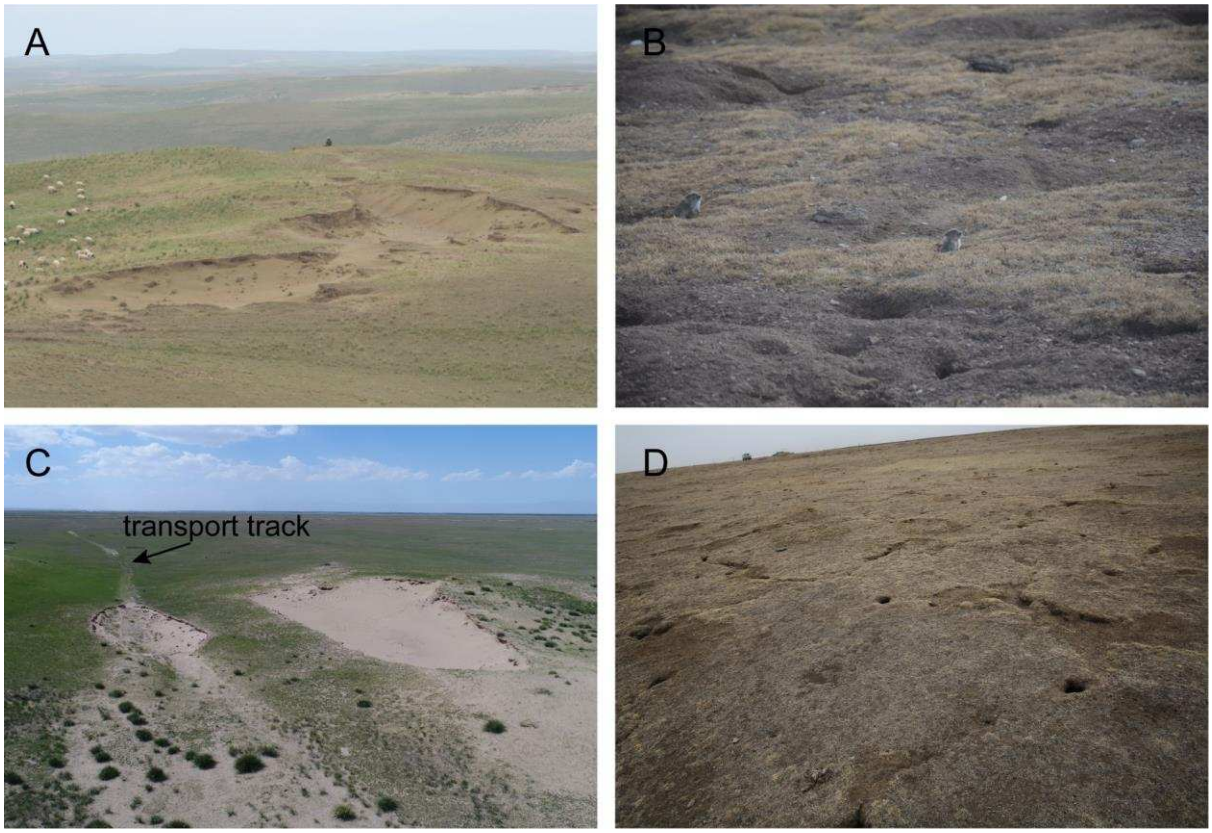

Figure 9. Factors triggering the surface disturbance and blowout formation. A) over grazing leading to two blowouts merging together; B. burrows of Pika as a serious disturbance of the grassland in QTP; C. vehicle tracks destroy the top surface vegetation layer and induce wind erosion along the track; D, freeze-thaw cycle cracked polygons on the top of grassland also providing conditions for wind erosion to occur in these gaps to form sand patches)

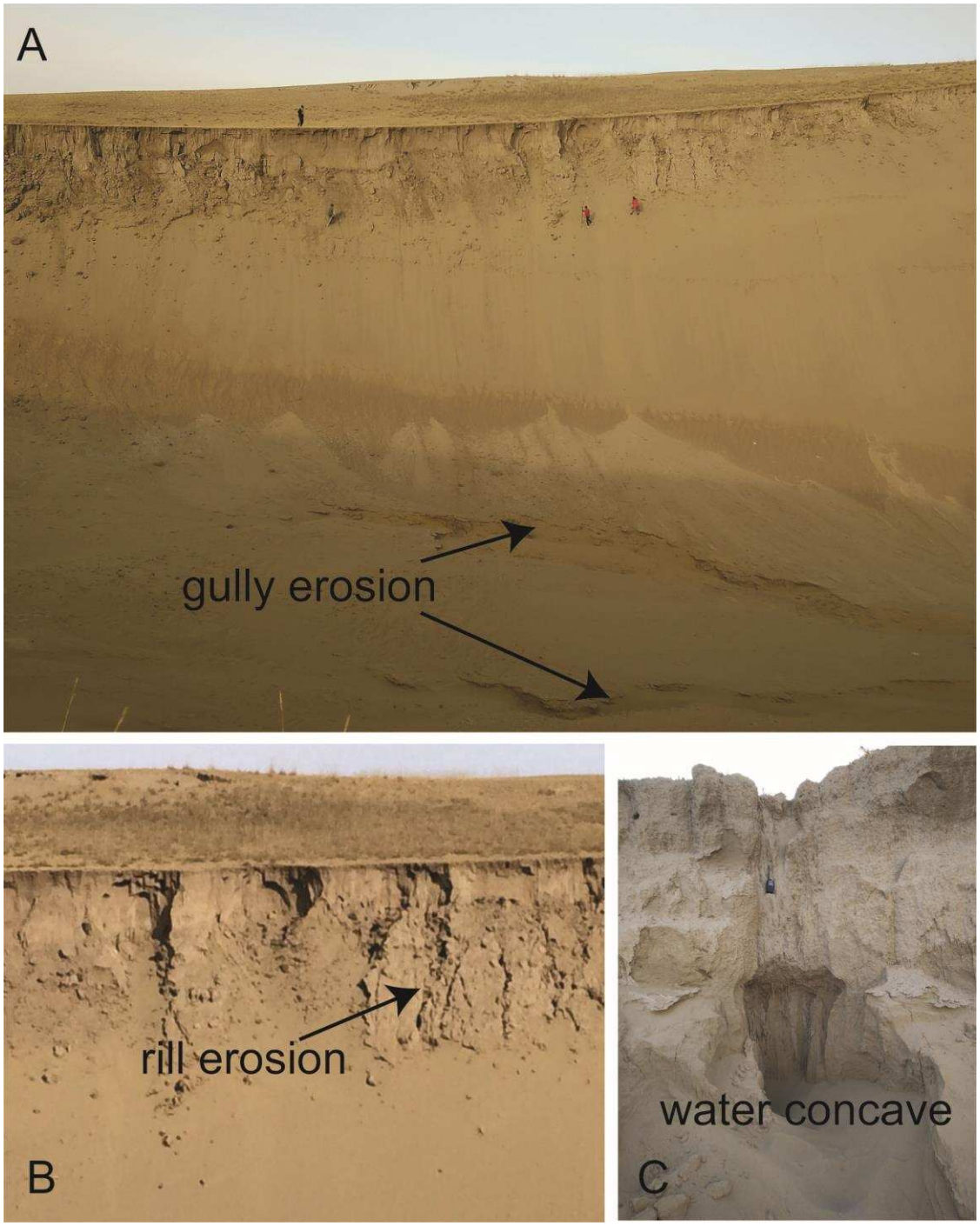

Figure 10. Gully erosion of the blowouts side wall and plain by a storm rain event in the rainy season. A). deflation plain gully erosion; B. side wall rill erosion; C. side wall concave water erosion)

Figure 11. Freeze-thaw cycle induced formation and evolution of blowouts in high altitude alpine regions in the Zogil basin. A. Freeze-thaw polygon B. freeze-thaw cavity C. freeze-thaw patches D. Patches merge, Sandy layer exposed E. Meadow disappeared and sand sheet spreading F. Severe wind erosion Blowout expansion)

Figure12. Freeze-thaw induced fracture and side wall collapse during the Spring season in Gonghe basin blowouts

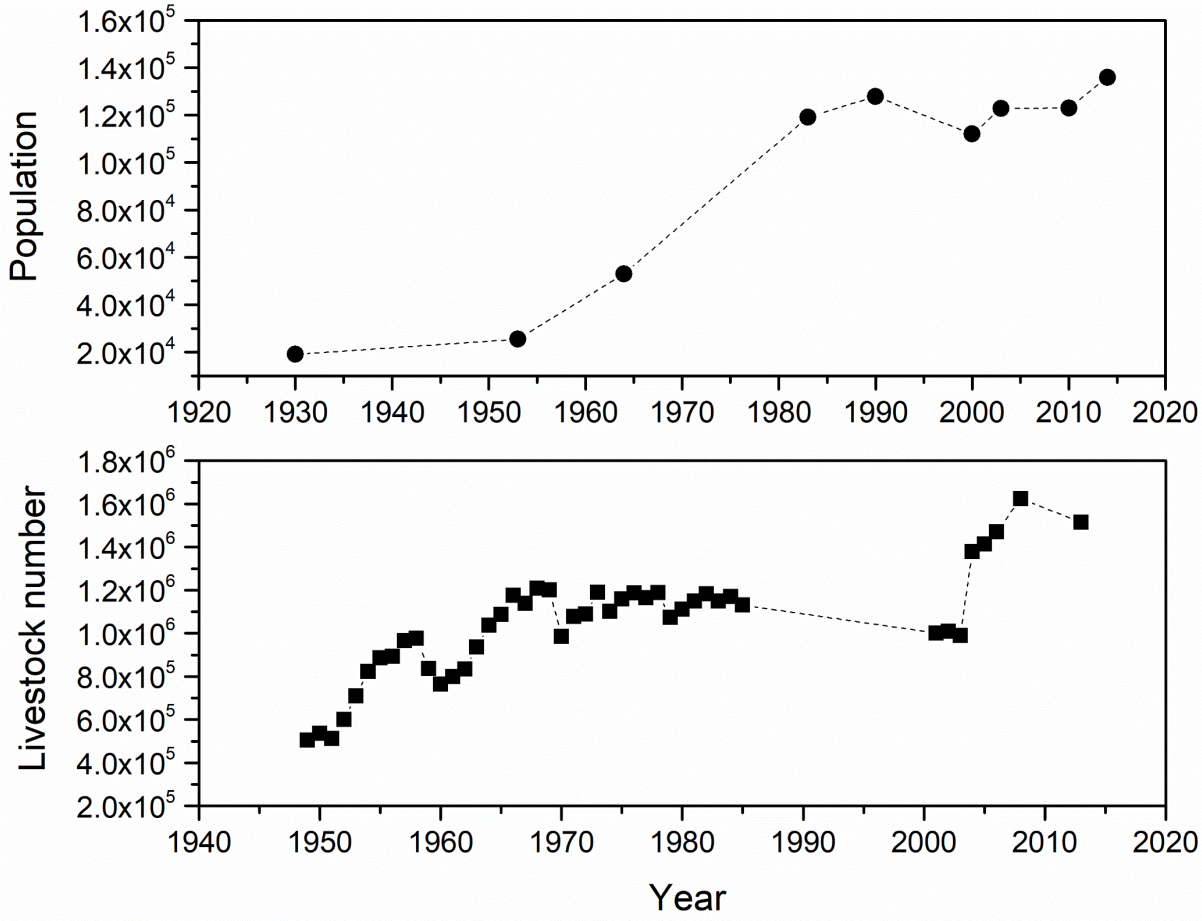

Fig. 13 Grazing capacity and population growth in the past decades in Gonghe